Japanese Journal of Applied Physics
Vol. 45, No. 1A, 2006, pp. 285–291

Electron–Photon Pulse Correlator Based on Space-Charge Effects in a Metal Pinhole

A. DOLOCAN, M. HENGSBERGER, H. J. NEFF, M. BARRY, C. CIRELLI, T. GREBER and J. OSTERWALDER

Physik-Institut, Universität Zürich, Winterthurerstr. 190, CH-8057 Zürich, Switzerland

(Received September 12, 2005; accepted October 7, 2005; published online January 10, 2006)

A new procedure is demonstrated for cross-correlating light and electron pulses in a time-resolved surface diffraction experiment using low-energy electrons: Ultrashort laser pulses produce a space charge that modulates the transmission of the electron pulses across a pinhole. The proposed method is easily implemented into present pump-probe setups and represents a simple means for establishing spatial and temporal overlap of light and electron pulses on the sample. Moreover, the ultrafast space-charge dynamics allow the temporal resolution of the electron pulses to be characterized down to a time scale of less than 20 ps. [DOI: 10.1143/JJAP.45.285]

KEYWORDS: ultrashort laser pulses, ultrashort electron pulses, ultrafast electron–photon correlation, ultrafast space-charge dynamics

1. Introduction

Over the last several years, time-resolved electron diffraction proved to be an excellent tool for obtaining information about structural dynamics in molecules and in condensed matter.[1–10] The basic experimental setup is common to all these studies: ultrashort laser pulses are split into two parts, one of them being used for initiating the process under investigation, while the second one generates the electron pulse on a back-illuminated metallic thin-film cathode. The temporal delay between the two is varied by controlling the optical path length. The bias potential of the cathode with respect to the potential of the sample defines the electron energy at the sample.

In surface science the necessity of high sensitivity to a few atomic layers and the Debye–Waller effect, suppressing diffraction intensities of diffraction spots with increasing temperature and electron momentum transfer, set constraints for electron energy and scattering angles. As a consequence, two main energy ranges are exploited: high kinetic energies typically ranging from about 15 to 100 keV where surface sensitivity is achieved by grazing incidence of the electrons onto the sample (RHEED), and low energies of 20 to about 300 eV (LEED). In the latter range, scattering angles are large and the low kinetic energy allows for spectroscopic analysis of the backscattered electrons. In conjunction with vast theoretical efforts for modeling LEED intensities[11] the technique has been by far the most successful structural tool in surface science. The achievement of ultra-high temporal resolution, however, is largely hampered by the low electron velocity and the increasing importance of space-charge effects within single electron pulses as well as path length differences (see, e.g., refs. 12 and 13). While at high energies the temporal resolution can be pushed into the range of a few hundreds of femtoseconds,[2,14] only theoretical estimates based on special gun designs can be found so far for low energies.[13]

Several practical problems arise when conducting time-resolved electron scattering experiments: First, spatial overlap has to be established between the pump light and the probing electron pulses precisely at the center of interaction, i.e., on the sample surface. This is a considerable task since the electron currents are of the order of pico- or even femtoamperes. Second, the coincidence time needs to be found, i.e., the delay of the two laser pulses for which electron and light pulses hit the surface at the same time. Both, spatial and temporal overlap should be established independently of the experiment itself. Furthermore, the electron pulse width, which usually limits the temporal resolution, has to be measured. Based on the forces exerted on the electronic charge by the vector potential of the light, one might think about a direct electron-light correlation experiment. In this way, one could take advantage of the femtosecond light pulse in order to map the electron pulse shape to a high degree of accuracy. In practice, however, such "slicing" experiments require a long interaction path and small velocity mismatch in order to obtain observable signal intensities. Such requirements are met in synchrotron storage rings.[15,16] In time-resolved electron scattering experiments, however, interaction volumes have to be kept small in order to maximize the temporal resolution owing to the high velocity mismatch.[17]

In gas-phase experiments, it was shown previously that the shape of the electron spot in high-energy diffraction experiments is changed due to Coulomb interaction of the electrons with plasma created by intense light pulses via photoionization.[4] In that case the plasma produced a positive electron-optical lens which focused the electron beam. Maximizing this effect allowed the spatial and temporal overlap of electron beam and pump light to be established inside the gas jet with an accuracy corresponding to the beam waist and to about 2 ps, respectively.[4,5] The temporal width of the electron pulses is then measured by streaking techniques which translate the time into a spatial dimension by deflecting the electron beam in a fast varying electric field.[5] Due to the difficulties in implementing the streak camera close to the center of interaction, the actual pulse width has to be inferred from streak measurements and numerical simulations of the pulse broadening during the electron drift[18] or else from the experimental results themselves.

The purpose of this paper is to demonstrate that spatial and temporal overlap can routinely be found in a very simple experiment similar to the procedure used previously,[4] but now applicable in a surface science experimental setup with no gas jet. Briefly, an aluminum plate is mounted beside the sample and at precisely the same distance from the electron gun. The electron beam is threaded through a pinhole in the plate and detected in transmission by a single-electron detector. The pump beam is focused into the pinhole and

produces a short-lived electronic space charge by multi-photon photoemission.[19] In coincidence, the flux of electrons transmitted through the pinhole changes due to the Coulomb interaction between the electrons in the pulses and the space charge. While the spatial overlap is determined by the pinhole itself, temporal coincidence is obtained by recording the transmitted electron yield as a function of the pulse delay. Moreover, the fastest feature observed in the transient transmission can be used to set an upper bound for the electron pulse duration, only limited by the surprisingly short lifetime of the space charge and irrespective of the electron energy.

2. Experimental Setup

The complete setup consists of two separate parts, the femtosecond laser system and the actual electron scattering experiment in an ultra-high vacuum chamber [Fig. 1(a)]. The heart of the laser system is a Coherent Mira Seed Ti:sapphire oscillator providing 800 nm pulses of 55 fs duration. The pulses are stretched and amplified by a regenerative amplifier (Coherent RegA 9050) and finally recompressed to about 65 fs (assuming Gaussian pulse shape) by means of a grating compressor. At the output of the compressor, the pulse energy is about 5 μJ at a repetition rate of 250 kHz. Part of the light is frequency-doubled in a β-bariumborate (BBO) crystal and separated from the residual pump light by a dichroic mirror. It is used for producing the electron probe pulse on a back-illuminated metal cathode. The residual light is delayed in order to compensate for the electron flight time and focused to a size of about 200 μm into the pinhole (pump pulse), as shown in Fig. 1(b). The pump beam is chopped with a frequency of about 1 Hz. This allows the data taken with pump light to be normalized to those taken without pump light. The length of the light path of the probe pulse and, thereby, the arrival time of the probe pulse with respect to that of the pump pulse is varied by means of a computer-controlled delay stage.

The vacuum system, with a base pressure in the low 10^{-9} Pa range, is equipped with standard surface science preparation and characterization facilities. Samples and the pinhole plate are mounted on a two-axes goniometer, described in detail in ref. 20. By simple linear motion the pinhole plate can be moved to the position of the sample for time-resolved electron diffraction experiments such that the pinhole entrance is precisely at the same distance from the gun as the sample. The plate is made out of 1 mm thick aluminium and contains pinholes which are 300 μm, 500 μm, and 1 mm in diameter. Behind the pinhole plate, a position-sensitive resistive-anode detector is mounted. The input signal of the detector is amplified by a double-microchannel-plate assembly that was demonstrated to be sensitive to single electrons from the gun.[13] A biased grid in front of the detector works as high-pass filter and prevents low-energy secondary electrons from reaching the detector. The assembly is shown in Fig. 1(b).

The intense pump pulse produces electrons in the pinhole via the photoelectric effect. For the given combination of low photon energy (1.55 eV) and high work function of the material (4.15 eV), multi-photon absorption is required.[19] The energy distribution of these photoelectrons was measured in a separate experiment, the results being shown in Fig. 2. The spectrum is characterized by a sharp onset at low energies and a broad structureless tail ranging up to 70 eV in kinetic energy. It has to be noted that the large space charge photoemitted by the intense laser pulse produces a electric dipole close to the surface, which shifts the spectrum to lower kinetic energies by a few hundreds meV. The kinetic energy zero was chosen such that it coincides with the onset measured in this spectrum. The average velocity of the photoelectrons was found to be 1.2×10^6 m/s for a fluence of about 10 mJ/cm^2, the total photocurrent was $\approx 8 \times 10^4$

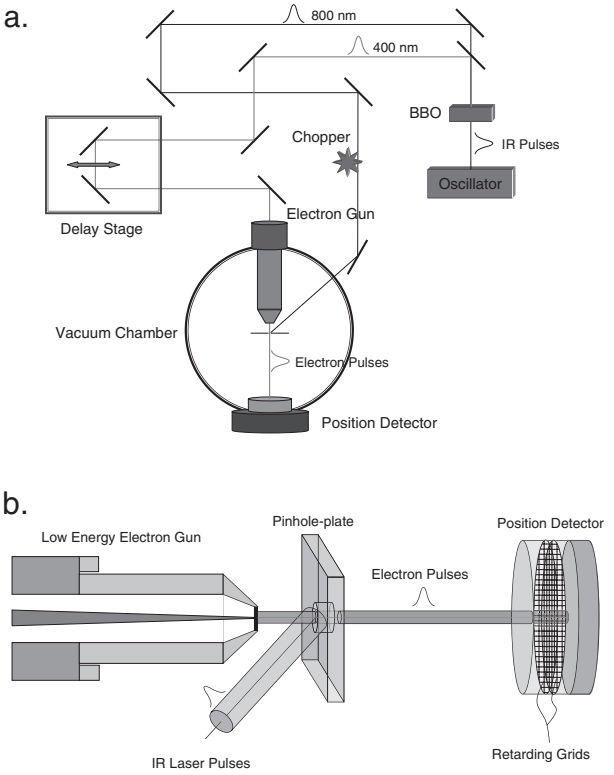

Fig. 1. (a) Experimental setup of the electron–photon correlation experiment. (b) Detailed view of the setup in the vacuum chamber with electron gun, pinhole plate, and electron detector.

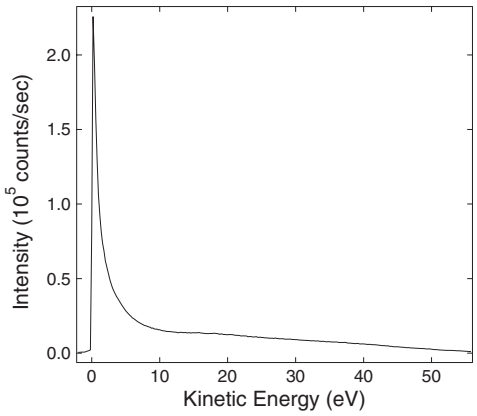

Fig. 2. Energy distribution of photoelectrons emitted from polycristalline aluminium by multi-photon absorption at a photon energy of 1.55 eV. The work function was measured to be 4.15 eV. The sample was biased at −10 V, the kinetic energy scale is referenced to the vacuum level. The fluence of the light is about 10 mJ/cm^2 in this case. The average velocity of the electrons in vacuum was determined to be $\langle v \rangle \approx 1.2 \times 10^6$ m/s.

electrons per laser shot or ≈3 nA. The resulting quantum efficiency, defined as the average number of photoelectrons per impinging photon amounts to $\eta \approx 4 \times 10^{-9}$ for this process.

The experiments were carried out with two different pulsed electron sources. The first one, referred to hereafter as LEED-gun, was developed for electron diffraction with high temporal resolution (5 ps) at low kinetic energies.[13,21] The head of this gun contains a gold film cathode on a mica substrate, which is separated from the anode through a kapton thin film spacer of $d = 75\,\mu$m thickness. The anode is an 800 μm thick microchannel plate, held on ground potential, which acts as collimator for the electrons. The distance between the cathode and the sample (here the pinhole) is about 4 mm which leads to an electron flight time of about 500 to 1000 ps for kinetic energies of the order of 100 eV. The electron beam diameter is ≈400 μm. The theoretical time spread of the electron pulses was calculated to be below 5 ps for an initial energy distribution of 1.2 eV, which is determined by the workfunction of gold and the employed photon energy of 3.1 eV.[13]

The second gun, referred to as MEED-gun, was originally designed for high- and medium-energy electron diffraction[22,23] and was operated here at low energy with re-optimized lens settings. The electrostatic lenses were adjusted using ray-tracing calculations[24] such that the electrons were accelerated to high kinetic energy (3 keV) directly after emission from the cathode and decelerated to their final kinetic energy at the exit of the gun. The total flight time of the electrons over the distance of roughly 34 cm from the cathode to the sample was, thereby, reduced from 44 to 27 ns. Based on the ray-tracing calculations, the final temporal spread of the electron pulses from the MEED-gun at the sample or pinhole plate was estimated to be of the order of 150 ps for excitation of electrons from the silver cathode using photons of 3.1 eV energy.

3. Experimental Data

In Fig. 3 an electron–photon correlation curve for electron pulses of 250 eV kinetic energy produced with the LEED-gun is shown. As long as the electron pulses arrive at the pinhole before the red laser pump pulses, the count rate measured behind the pinhole is constant (normalized to unity). Near the coincidence point we see a sharp drop by about 20% of the electron count, a slightly slower recovery, and a weaker, more extended ringing for longer electron delays. This demonstrates clearly that we observe an interaction between the pump light and the electron pulses mediated by the transient space charge in the pinhole.

The curves were fitted in two different ways (see Fig. 3) in order to quantify time scales (bottom curve), or to get further insight into the interaction processes of the electron pulses with the space charge (top curve). In the first approach, the leading edge is fitted by a step function of the Fermi–Dirac type. The rise time (or here rather "drop time") Δt is defined as the time interval over which the Fermi–Dirac function drops from 90 to 10% of its maximum step height. For this particular data set we obtain a value of $\Delta t \leqslant 20$ ps, which is the shortest feature ever observed in our experiments. The count rate recovery is fitted with a simple exponential of negative amplitude, from which a

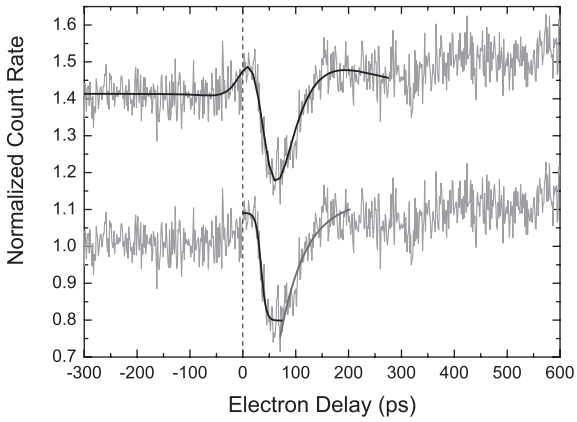

Fig. 3. Electron–photon correlation curve for electron pulses of 250 eV kinetic energy produced with the LEED-gun. The red laser power impinging on the 500 μm diameter pinhole was ≃0.9 W. The data have been normalized for each delay by the corresponding count rate without pump light on the pinhole. The same measurement is plotted twice in order to illustrate two different fitting functions for describing the correlation signal (see text). The upper curve has been simply offset.

recovery time τ of 50 ps results. The weak oscillations at longer delays have not been further analyzed. Since the measured drop time Δt results from a nontrivial convolution (in space and time) of the electron pulse shape and the temporal profile of the space charge formation, the value of 20 ps gives an upper limit for both.

For a simple model of the space charge dynamics, we use the value for the mean velocity $\langle v \rangle \approx 1.2 \times 10^6$ m/s of the electrons produced by the pump pulse. Again, this has to be taken as upper limit since kinetic energy is redistributed within the space charge during the flight owing to Coulomb interaction between the electrons.[18] Since this effect broadens the energy spectrum, the initial energy distribution is expected to be piled up at lower kinetic energies. The value of the average velocity given above corresponds to the velocity of the center of gravity of the space charge in one dimension.[25] During the maximum space-charge build-up time (taken as $\Delta t = 20$ ps) the electrons travel with this energy a distance of 23 μm, which means that they have only the time to form a ring of charge around the 500 μm diameter pinhole.[26] During the recovery time of 50 ps they travel an additional 58 μm. If one assumes that the electron cloud forms half a torus centered on the pinhole axis, the thickness of which grows with time (with a volume $V(t) = \pi^2[r(t)]^2 R$, where $R = 250\,\mu$m is the radius of the pinhole) then one can compute the mean electron density as a function of time: $1.8 \times 10^{-2}\,\mathrm{C/m^3}$ ($r = 23\,\mu$m) after the 20 ps space-charge build-up time and $1.5 \times 10^{-3}\,\mathrm{C/m^3}$ ($r = 81\,\mu$m) after the 50 ps relaxation. The density is about one order of magnitude higher after the build-up part which shows that the electron cloud disperses quite fast over a time scale of 50 ps. From our data we conclude that the electrostatic potential built by the space-charge has a maximum influence on the electron beam when it is concentrated on a radius of about 50 μm around the pinhole edge.

Before the second approach to fitting the correlation curve (top curve of Fig. 3) is discussed, we show in Fig. 4 the electron–photon correlation curves for different electron energies, i.e., cathode potentials in the LEED-gun. All

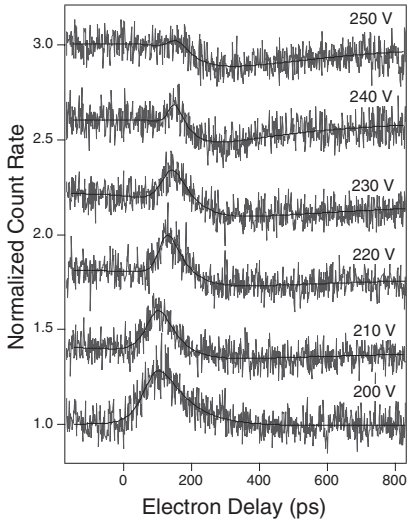

Fig. 4. Electron–photon correlation curves for electron pulses of 200 to 250 eV kinetic energy produced with the LEED-gun. The pinhole diameter was 300 μm, the red laser power ≃0.5 W. The delay times are referenced to some arbitrary but fixed position of the delay line. All curves except for the lowest one have been offset by an increasing amount. The fits represented by the solid lines are discussed in the text.

curves show a correlation signal, but the shape changes dramatically with the electron energy. While there is again a marked drop ($\simeq -11\%$) of electron transmission through the pinhole at 250 eV, an effect we term *shielding*, the opposite behavior is observed for 200 eV electrons: the transmission increases by $\simeq +27\%$ near the coincidence point. Accordingly, we term this effect *lensing*. There is a gradual change from lensing to shielding behavior with increasing energy. Likewise, there is a gradual shift of the onset of the leading edge to later delay times. This latter effect is related to the increasing speed of the electrons. In order to coincide with the red laser pump pulse (which fixes the delay axis) at the pinhole, faster electrons must be produced later at the photocathode, i.e., there is a right-shift of the onset with increasing energy.

The observation of both shielding and lensing effects in the correlation curves raises the question as to how the shape and the dynamics of the space-charge cloud influences the electron trajectories and thus the transmission of the electron beam. In §4 it is briefly discussed that reasonable static space-charge distributions can be constructed to produce either shielding or lensing. We take this as a justification for introducing a pragmatic model for the space-charge dynamics and its effects on the pinhole transmission, leading to the second type of fitting function to the correlation curves (Fig. 3, upper curve). Let $\rho_L(\mathbf{r})$ be a static charge distribution at the pinhole that leads to lensing and $\rho_S(\mathbf{r})$ one that leads to shielding. Let us further assume that $\rho_L(\mathbf{r})$ and $\rho_S(\mathbf{r})$ can be found such that the actual space-charge cloud $\rho(\mathbf{r}, t)$ can be represented for any time t as a linear combination of the two: $\rho(\mathbf{r}, t) = c_L(t)\rho_L(\mathbf{r}) + c_S(t)\rho_S(\mathbf{r})$. Due to the linearity of Poisson's equation and the equations of motion, this charge distribution should, to first order, produce the observed combination of lensing and shielding effects observed in our experiment. The model neglects truly dynamical effects arising due to time-dependent electric fields. The time-dependent coefficients are represented by a leading edge, represented as a Fermi–Dirac function (τ_1^L, τ_1^S), multiplied by an exponential decay (τ_2^L, τ_2^S), providing an excellent description of the shielding (lensing) case alone (Fig. 4, top and bottom curves). The complete fitting function for the normalized electron transmission through the pinhole, where $N_0 + \Delta N(t)$ and N_0 are the numbers of transmitted electrons in the presence or absence of pump beam pulses, respectively, is then:

$$\frac{N_0 + \Delta N(t)}{N_0} = A_L c_L(t) - A_S c_S(t) + 1 = \frac{A_L e^{-(t-t_0)/\tau_2^L}}{1 + e^{-(t-t_0)/\tau_1^L}} - \frac{A_S e^{-(t-t_0)/\tau_2^S}}{1 + e^{-(t-t_0)/\tau_1^S}} + 1 \quad (1)$$

with A_L and A_S describing the amplitude of the lensing and shielding effect, respectively. t_0 defines the rising/falling edge position. In order to limit the number of free parameters, one common parameter t_0 is used for both effects.

As is evident from Figs. 4 and 3 (upper curve) this function provides an excellent description of all data. For the data of Fig. 4 the resulting fitting parameters can be used to analyze the interaction of the electron beam with the space charge. From a linear regression to values of the edge position t_0 versus the inverse of the electron velocity we obtain a slope of 5.21 mm, which relates to the electron drift distance from the photocathode to the pinhole plate. It is in good agreement with the geometrical distance of about 4 mm, considering that this analysis neglects the acceleration of the electrons between cathode and anode. Over the voltage range from 200 to 250 eV, the lensing amplitude A_L drops from about 0.51 to 0.28, while A_S increases from 0.01 to 0.25. Since the lensing and shielding functions are not normalized, these amplitudes do not reflect the visual impression that at 250 V there is essentially shielding only. Unfortunately, it is found that the characteristic times τ_1^L, τ_2^L, τ_1^S, τ_2^S are rather interdependent and do not allow for an unambiguous description of the space charge dynamics. The most stable of these parameters is τ_1^L which describes the width of the leading lensing edge. It is found to decrease gradually from 21 to about 13 ps over the measured voltage range. This narrowing of the edge reflects the change of the temporal width of the electron pulse that probes the space charge region and the time (and distance) over which this pulse is affected by the space charge.

Due to the interdependence of the characteristic times in this model we revert to the simpler edge-fitting procedure described earlier (Fig. 3, bottom curve) for a discussion of the fastest temporal change appearing in the curves around the coincidence point, i.e., the leading edge, and its dependence on various experimental parameters. Note that the edge time-width Δt for the 90–10% drop time of a Fermi–Dirac function (proportional to $1/(1 + \exp -(t - t_0)/\tau_1)$) corresponds to about $4.4 \times \tau_1$. In Fig. 5 we give these width Δt as a function of electron energy. There is a systematic narrowing of the edge with increasing energy suggesting that the edge width is an indicator for the electron pulse width. The large scatter in these values show how sensitive the correlation curves are to the spatial alignment of the pump and probe pulses with respect to the pinhole and to each other. Reproducibility was thus a serious issue in these experiments, which is indicated in the figure by the

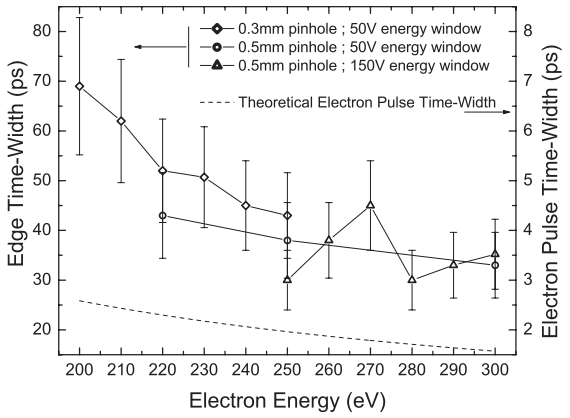

Fig. 5. Compilation of the leading edge temporal widths from most of the electron–photon correlation data measured for the LEED-gun. As indicated by the legend, some curves have been measured with a 300 μm diameter pinhole (◇), some with 500 μm (○, △). In the former case, the detector energy window (see text) was 50 eV, in the latter case either 50 eV (○) or 150 eV (△). The error bars reflect the scatter of values obtained in repeated measurements. The dashed line indicates the theoretical value for the expected temporal spread of the electron pulse due to the non-monochromaticity ($\Delta E = 1.12$ eV) of the beam.

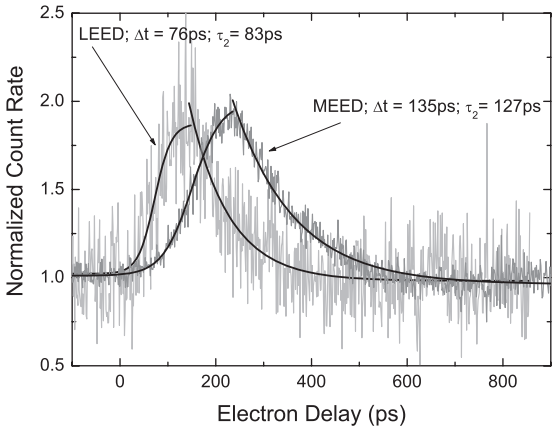

Fig. 6. Comparison of electron–photon correlation curves for electron pulses of 200 eV energy produced by the LEED-gun or by the MEED-gun, using the 300 μm diameter pinhole. The red-laser pump power was 0.9 W in both cases, the detector energy window was set to 50 and 5 eV for the LEED-gun and MEED-gun, respectively. The simple edge-fitting method was applied in order to extract the characteristic temporal parameters.

large error bars. Another issue is that the edge widths are larger than the pulse widths theoretically expected for the LEED-gun by more than an order of magnitude. In taking into account only the effect of non-monochromaticity of the electrons ($\Delta E = 1.12$ eV[13]) we expect a time spread

$$\Delta t \approx \frac{\sqrt{m}}{2eV_0}\left(\frac{d}{\sqrt{2E}} + \frac{L}{\sqrt{2eV_0}}\right)\Delta E, \qquad (2)$$

from which we obtain pulse widths as indicated by the dashed curve in Fig. 5. Here, d and L are the cathode–anode distance and the drift distance to the sample, respectively, V_0 is the cathode (or acceleration) voltage and E is the initial energy at the photocathode, here taken as $E = \Delta E/2 = 0.56$ eV, and m is the electron mass. Expression (2) holds for $\Delta E \ll eV_0$. The measured edge widths are much larger than the theoretically expected ones, though they follow the expected energy dependence. The edge width depends in a complex way on the time constants of the transient electric field produced by the space charge in the pinhole and the pulse width of the electron pulse. Further experiments and numerical simulations will be needed to disentangle these time broadening effects. Owing to the energy dependence of the observed edge width, it is likely that the electron gun makes the dominant contribution to the temporal resolution. Nevertheless, it has to be emphasized that this is the first time that such high temporal resolution has been achieved with electrons at low kinetic energy.

Energy resolution on the detection side is an efficient means for increasing the temporal resolution. This can be seen by analyzing correlation curves measured with different potentials at the retarding grids of the two-dimensional detector. For 250 eV electrons the edge width drops from ~120 ps at 50 V retarding potential to ~200 ps at 230 V. In the latter case, the energy window seen by the detector is reduced to 20 eV and most of the inelastically scattered and secondary electrons, produced either in the LEED-gun or in the pinhole, are suppressed.

In order to create a situation where the time scale of the correlation signal is clearly dominated by the width of the electron pulses, we carried out similar experiments with the MEED-gun that produces much longer electron pulses when used in the low-energy range. In Fig. 6 correlation curves for the two guns are compared for an electron energy of 200 eV. Due to the much higher beam current of the MEED-gun, the detector window could be reduced to 5 eV in this case. Nevertheless, the edge width for these pulses is significantly larger than that from the LEED-gun. At least in the leading edge, the curve provides a good measure of the temporal profile of the electron pulses. The width of the rising edge is $\Delta t = 135$ ps which is in good agreement with a value of 144 ps obtained from ray tracing calculations for the MEED-gun. The rise-time Δt and the decay time τ_2 are very similar suggesting that the electron–photon correlation function is dominated by the time resolution of the MEED-gun. When the electron energy of the MEED-gun pulses is varied, similar effects are observed as those seen with the LEED-gun (Fig. 4): with increasing energy the leading edge shifts to later delays and the edge width narrows, and the general behavior transforms from lensing to shielding. The temporal shifts are much larger in this case due to the long electron path lengths in this gun.

One means for manipulating the space charge and its dynamics is to vary the power of the red pump pulses. As Fig. 7 shows impressively, the correlation curve changes dramatically when the pump power is roughly doubled. The behavior shifts from shielding to lensing, with a strong increase of the overall effect (+110% versus −11%), and with a slight increase in the edge width. Increasing the pump power not only multiplies the number of electrons in the space charge cloud, it also increases the effective pump-beam cross section at the pinhole, and thus the volume of the space charge. The mechanism leading to the drastic changes in the correlation curves is not clear. It cannot be elucidated without a detailed modeling of the space charge dynamics and its effects on the electron beam trajectories, which is beyond the scope of this paper. However, these strong effects must be responsible for the large scatter and poor

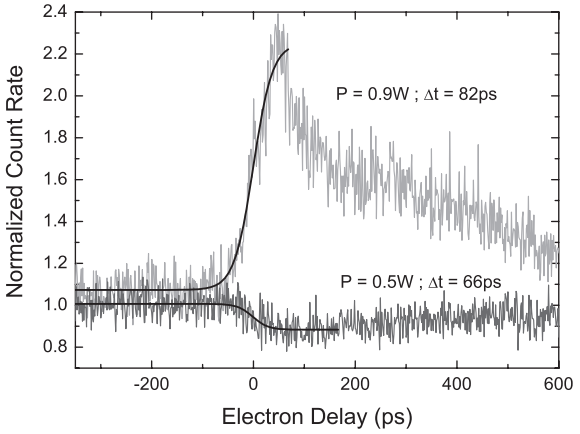

Fig. 7. Influence of the red laser pump power on the electron–photon correlation curve for LEED-gun pulses of 250 eV energy. The two curves were measured back to back, with pump powers of 0.9 W (upper curve) and 0.5 W (lower curve) on the 300 µm diameter pinhole. The leading edges were fitted with Fermi–Dirac functions to determine the 90 to 10% drop (rise) times Δt.

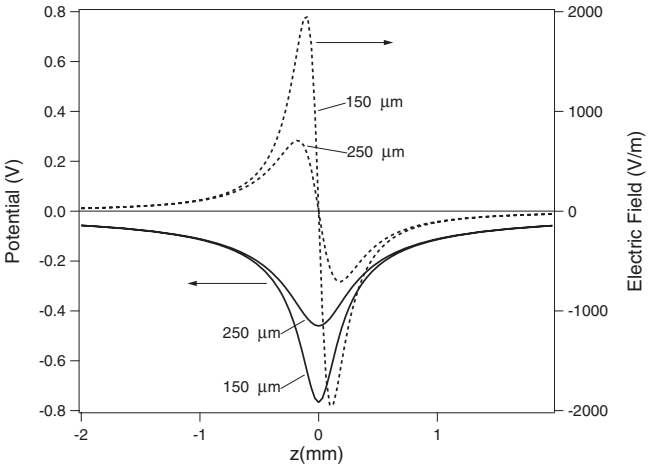

Fig. 8. Calculated potential and electric field for $R = 150$ and 250 µm (with Q_0 estimated from the aluminium spectrum of Fig. 2).

reproducibility of correlation curves that we have seen in the course of these experiments.

In a pragmatic sense we can give the following recommendations for the use of this pinhole-based electron–photon pulse correlator: By maximizing the overall effect that the electron pulses see from the pinhole, one can optimize the spatial overlap of red laser pump and electron probe pulses and find the temporal coincidence time at the pinhole. At least down to the time scale of the order of 20 ps, as demonstrated here, the temporal profile of the electron pulses can be characterized. Replacing the pinhole-plate with a sample by a simple linear translation, one can perform other electron–photon correlation experiments, such as, e.g., time-resolved LEED, with the significant advantage of having previously established spatial and temporal overlap on the sample surface. Even though the temporal profile of the electron pulses cannot be characterized as precisely as with a streak-camera, the information is sampled at the position of interest and not after some distance where further temporal spread occurs that has to be taken in consideration for the retrieval of the true pulse width. We also would like to emphasize that the space charge following the absorption of intense laser pulses in pump-probe experiments may also occur in electron scattering experiments. This effects should thus be considered carefully during the analysis of any time-resolved experiments involving electrons.

4. Theoretical Notes and Simulations

The non-trivial combinations of lensing and shielding effects seen in the correlation experiments are not easy to understand in detail. They are obviously related to the energy and to the temporal spread of the electron pulses as well as the space-charge dynamics, the details of which are beyond the scope of this work. Nevertheless we attempt to have some insight into the mechanisms for the two effects from simple electrostatic arguments. The simplest way to put the problem is to consider the space-charge as an infinitely thin circular charge distribution with radius R at the pinhole entrance. The potential along the pinhole axis z is then easily calculated as

$$\Phi(z) = \frac{Q_0}{4\pi\epsilon_0\sqrt{R^2 + z^2}}. \tag{3}$$

Here, Q_0 is the total amount of charge on the circle that can be approximated by the total charge excited by one red laser pump pulse, which was estimated to be 8×10^4 electrons for aluminium as the pinhole material (see §2).

Figure 8 shows the potential as well as the electric field along the central axis for the 300 µm and the 500 µm diameter pinholes. The potential values reached on the axis are less than 1 V. At electron energies of the order of 200 eV we thus expect the main effects arising at the fringes of the pinhole, not at the center. This is confirmed by ray tracing calculations using cylindrical symmetry and a similarly simple charge distribution at the pinhole entrance that produces a focussing of the beam near the pinhole axis while trajectories near the rim are rejected that would pass through the pinhole in the absence of an electric field (thus *shielding*). However, these simulations cannot explain the large magnitude of the shielding effect (up to 20%).

The lensing effect is even harder to explain. In this simple potential geometry, the only way to obtain lensing in ray tracing calculations was by threading the beam with some tilt angle relative to the axis through the pinhole. Basically, the space charge potential can then help to steer electrons through the pinhole. In the real experimental geometry the situation arises more likely due to some lateral misalignment of the electron beam with the pinhole, and due to the oblique incidence of the pump beam onto the pinhole. Situations can then be constructed where the repulsive space charge potential pushes more electrons into the pinhole (thus *lensing*).

Overall, the large magnitudes observed for both lensing and shielding effects can only be understood as a consequence of a strong perturbation of axial symmetry of the space charge geometry arising from the oblique incidence of the pump beam onto the pinhole. Subtle changes in the alignment of electron and pump beam with respect to each other, and to the pinhole, thus lead to dramatic changes in electron transmission, explaining also the difficulty in reproducing exactly the same correlation curves in repeated experiments. Since this alignment is likely changed by small

amounts in varying parameters like electron energy or pump beam power, systematic changes in the shape of the correlation curves, like those observed in Figs. 4 and 7, must not necessarily reflect significant changes in the space charge dynamics but more trivial geometrical effects. Nevertheless, the time scale provided by the leading edge should still be a measure for the electron pulse width and the space charge build-up time.

5. Conclusions

A device based on electron transmission through a pinhole is demonstrated for establishing temporal and spatial correlation for low-energy electron pulses and laser pulses. It is easily implemented in a pump-probe electron diffraction experiment and can be used for electron beam characterization at the site of the sample in a surface diffraction chamber. Down to a time scale of 20 ps the leading edge in the temporal correlation curve for electron transmission through the pinhole versus pump-probe delay provides information about the pulse width of the electron beam.

It is anticipated that this simple experiment may have further applications. As an example, the spatial intensity distribution and the beam divergence of the electron beam can easily be measured by using the pinhole as an aperture and recording the transmitted intensity as a function of transverse and longitudinal position of the pinhole with respect to the electron gun. As a more far-reaching application, one might even take advantage of the lensing effect by slightly misaligning a *continuous* electron beam with respect to the pinhole and to create picosecond electron bunches behind the pinhole by slicing the beam due to interaction with the short-lived space charge produced by the laser pulse.

Moreover, the two-dimensional electron detector used in this experiment lends itself for further characterization of the electron beam, but it can easily be replaced by a single channeltron detector for this type of correlation experiments, making the whole setup cheap and simple.

Acknowledgments

Financial support from the Swiss Science Foundation SNF through grants no. 200020-100471 and no. 59906 (CERC-3) and from the Research Foundation of the University of Zurich is gratefully acknowledged.

1) X. Zeng and H. E. Elsayed-Ali: Phys. Rev. B **64** (2001) 085410.
2) B. J. Siwick, J. R. Dwyer, R. E. Jordan and R. J. D. Miller: Science **302** (2003) 1382.
3) S. Williamson, G. Mourou and J. C. M. Li: Phys. Rev. Lett. **52** (1984) 2364.
4) M. Dantus, S. B. Kim, J. C. Williamson and A. H. Zewail: J. Phys. Chem. **98** (1994) 2782.
5) J. C. Williamson, J. Cao, H. Ihee, H. Frey and A. H. Zewail: Nature **386** (1997) 159.
6) H. Ihee, J. Cao and A. H. Zewail: Chem. Phys. Lett. **281** (1997) 10.
7) H. E. Elsayed-Ali and G. A. Mourou: Appl. Phys. Lett. **52** (1988) 103.
8) H. E. Elsayed-Ali and J. W. Herman: Appl. Phys. Lett. **57** (1990) 1508.
9) X. Zeng, B. Lin, I. El-Kholy and H. E. Elsayed-Ali: Phys. Rev. B **59** (1999) 14907.
10) C.-Y. Ruan, F. Vigliotti, V. A. Lobastov, S. Chen and A. H. Zewail: Proc. Natl. Acad. Sci. **101** (2004) 1123.
11) J. B. Pendry: in *Low Energy Electron Diffraction*, ed. G. K. T. Conn and K. R. Coleman (Academic Press, London and New York, 1974) Techniques of Physics Series.
12) J. R. Thompson, P. M. Weber and P. J. Estrup: Proc. SPIE **2521** (1995) 113.
13) R. Karrer, H. J. Neff, M. Hengsberger, T. Greber and J. Osterwalder: Rev. Sci. Instrum. **72** (2001) 4404.
14) H. Ihee, V. A. Lobastov, U. M. Gomez, B. M. Goodson, R. Srinivasan, C.-Y. Ruan and A. H. Zewail: Science **291** (2001) 458.
15) A. A. Zholents and M. S. Zolotorev: Phys. Rev. Lett. **76** (1996) 912.
16) R. W. Schoenlein, S. Chattopadhyay, H. H. W. Chong, T. E. Glover, P. A. Heimann, C. V. Shank, A. A. Zholents and M. S. Zolotorev: Science **287** (2000) 2237.
17) J. C. Williamson and A. H. Zewail: Chem. Phys. Lett. **209** (1993) 10.
18) B. J. Siwick, J. R. Dwyer, R. E. Jordan and R. J. D. Miller: J. Appl. Phys. **92** (2002) 1643.
19) J. G. Fujimoto, J. M. Liu, E. P. Ippen and N. Bloembergen: Phys. Rev. Lett. **53** (1984) 1837.
20) T. Greber, O. Raetzo, T. J. Kreutz, P. Schwaller, W. Deichmann, E. Wetli and J. Osterwalder: Rev. Sci. Instrum. **68** (1997) 4549.
21) R. Karrer: Diploma Thesis, University of Zürich, Switzerland, 2000 [in German].
22) M. Aeschlimann, E. Hull, J. Cao, C. A. Schuttenmaer, L. G. Jahn, Y. Gao, H. E. Elsayed-Ali, D. A. Mantell and M. R. Scheinfein: Rev. Sci. Instrum. **66** (1995) 1000.
23) M. Aeschlimann, E. Hull, C. A. Schmuttenmaer, J. Cao, Y. Gao, D. A. Mantell and H. E. Elsayed-Ali: Proc. SPIE **2521** (1995) 103.
24) SIMION 3D 7.0 software package, Idaho National Engineering Laboratory, EG&G Idaho Inc., Idaho Falls.
25) Employing a simple one-dimensional model here is justified because all relevant length scales are smaller than the lateral size of the beamwaist of the pump laser.
26) For reasons of tractability, we assume in this discussion a cylindrical symmetry around the pinhole axis, neglecting the strong perturbation of this symmetry by the oblique incidence of the pump beam onto the pinhole.